

铌酸锂混合集成波导非线性太赫兹源

王能宇,薛飞鸿,马晓飞,盛冲,肖彦玲,祝世宁,刘辉*

南京大学物理学院固体微结构物理国家重点实验室,人工微结构科学与技术协同创新中心,江苏南京210093

摘要 理论设计了光波-太赫兹波混合波导,构建了一种室温、连续、高效、集成化、低噪声、易于调制的相干太赫兹源。该混合波导由铌酸锂退火质子交换波导与金属超晶格波导混合集成,近红外通信波段的信号光和泵浦光在退火质子交换铌酸锂波导中传播,通过非线性差频产生0.379 THz的太赫兹波,所产生的太赫兹波通过金属超晶格波导传输。通过优化金属超晶格太赫兹波导的结构参数,理论上实现了准相位匹配,提高了太赫兹波的群折射率,从而通过慢光效应进一步增强非线性效应,理论非线性转换效率可达 $3.6 \times 10^{-7} \text{ W}^{-1}$ 。同时,所设计的混合集成波导结构也可用于其他非线性光学器件中。

关键词 铌酸锂; 波导; 超材料; 差频; 太赫兹

中图分类号 O436 **文献标志码** A

DOI: 10.3788/AOS240861

1 引言

近年来,第五代(5G)无线通信网络取得了显著进展。然而,随着全球无线数据流量的爆炸性增长,5G通信面临着无法满足这种指数增长需求的重大挑战。因此,下一代无线通信网络预计将极大地增加带宽以填补这一空缺。在这一背景下,太赫兹(THz)无线通信被视为6G网络的有力候选者^[1]。太赫兹频段位于微波和红外光波范围重叠的中间地带,被称为“太赫兹间隙”。它之所以被称为“间隙”,是因为其产生和操控的技术仍处于初期阶段。此外,太赫兹频段由于其安全、高速、稳定、穿透等独有特性,已被应用到多个领域,包括但不限于安全检测^[2]、生物医学成像^[3]、无线通信^[4-5]以及材料特性分析^[6]等。

当前,太赫兹科学与技术的快速发展遇到瓶颈,主要原因是传统的电子设备已无法满足具有高速调制特性和低噪声太赫兹波的产生需求。这一挑战阻碍了太赫兹技术在各个领域的广泛应用和商业化进程。目前,太赫兹辐射源主要分为两类^[7]:1)基于电子学技术的太赫兹辐射源,主要包括传统固态倍频源、太赫兹量子级联激光器、自由电子激光器、自旋太赫兹源^[8-9]等,这些都是毫米波和微波技术向短波方向的扩展。这类太赫兹辐射源的缺点是工作频率不高,难以调谐,难以适应下一代通信技术发展的需求^[10]。2)基于光子学技术的太赫兹辐射源^[11],主要包括等离子体、光电导效应、光整流效应、光学拍频、非线性光学差频等辐射源。

这是激光技术向长波方向的延伸,这类太赫兹辐射源的频谱范围较宽,输出功率较大,易于调制与进一步小型化和集成化,以及降低成本后具有很大的应用潜力。

在众多非线性产生太赫兹波的光学材料中,铁电材料铌酸锂(LN)由于具有优异的电光、声光与非线性特性,以及超宽的透明窗口和相对较高的折射率,成为最通用和最具吸引力的光子学材料之一^[12-17]。哈佛大学Marko Lončar教授曾预言:“10年内,薄膜铌酸锂将在所有高性能光电子应用中取代硅基光子,特别是在数据通信中!”铌酸锂材料具有很高的二阶有效非线性极化率,以及稳定的物理化学性质^[18],经过掺杂,可以制造出具有高激光损伤阈值的大晶体。基于铌酸锂材料的太赫兹源在产生高质量的光束方面更有效,稳定性更高,便于制备低噪声和易于调制的器件,用途广泛。早在1971年,加利福尼亚大学伯克利分校沈元壤教授课题组就用铌酸锂晶体产生了世界上第一个太赫兹脉冲辐射^[19]。但是激光和太赫兹辐射在铌酸锂材料中的折射率存在巨大差异(光学频段折射率约为2.3,太赫兹频段折射率约为4.9),因此光波和太赫兹波之间的相位失配严重,产生太赫兹辐射的非线性转化效率很低。

超材料通过人工设计的亚波长微结构,表现出许多天然材料所不具备的超常物理性质,在调控光学材料方面提供了前所未有的灵活性^[20]。超材料具有很多独特和引人注目的属性,产生了很多前所未有的应用,

收稿日期: 2024-04-17; 修回日期: 2024-05-19; 录用日期: 2024-05-27; 网络首发日期: 2024-05-28

基金项目: 国家重点研发计划(2023YFB2805700)、国家自然科学基金(12334015, 92163216, 92150302, 62288101)

通信作者: *liuhui@nju.edu.cn

如完美透镜^[21-22]、隐形斗篷^[23]、人造黑洞^[24]等。超材料的出现也为非线性光学的发展注入了新的活力^[25-27]。最近的研究中,超材料可以实现无相位失配的四波混频^[28],形成自相位调制和孤子波^[29],实现对太赫兹波相位和偏振态的操控^[30],通过构造跨波段的零折射率导波提升非线性转换效率^[31]。

本文提出一种由铌酸锂退火质子交换波导与金属超晶格波导混合集成的光波-太赫兹波混合波导结构,用于非线性光学差频产生(DFG)太赫兹波。利用金属超晶格对太赫兹电场的周期调控理论上可以实现准相位匹配,并且超晶格波导具有微带的色散特性和亚波长尺度的太赫兹模场分布,可以显著提升非线性耦合系数。

2 结构设计与模拟分析

在混合波导中,光通信波段(1260~1625 nm)内两束波长相近的近红外光可通过非线性差频作用产生太

赫兹波。考虑到0.35~0.44 THz波段太赫兹波的大气吸收较弱,适合用于无线通信,因此本实验产生0.378 THz的太赫兹波。由于太赫兹波与近红外光的波长相差较大,其折射率也相差较大,因此支持太赫兹波传播的波导与光波导也存在较大差异,需要两种不同的材料混合集成^[32]来分别传播近红外光波与太赫兹波。如图1所示,在所设计的结构中,退火质子交换铌酸锂(APELN)波导提供了对光波的强约束与超高的二阶非线性系数,用来传播两束信号光与泵浦光,并且产生差频。为了调控太赫兹波的传播,将两个周期性锯齿状的金属超晶格太赫兹波导等间距地相对放置在铌酸锂波导上,间距 $g=6 \mu\text{m}$,厚度 $h_{\text{Au}}=0.5 \mu\text{m}$,锯齿深度为 t 。金属超晶格太赫兹波导不仅引导太赫兹波的传播,还将太赫兹光场进行亚波长压缩,从而扩大太赫兹光场与铌酸锂光波导电场分布的空间交叠范围,进而增强非线性相互作用,最终差频产生的太赫兹波在波导的末端被辐射到自由空间中。

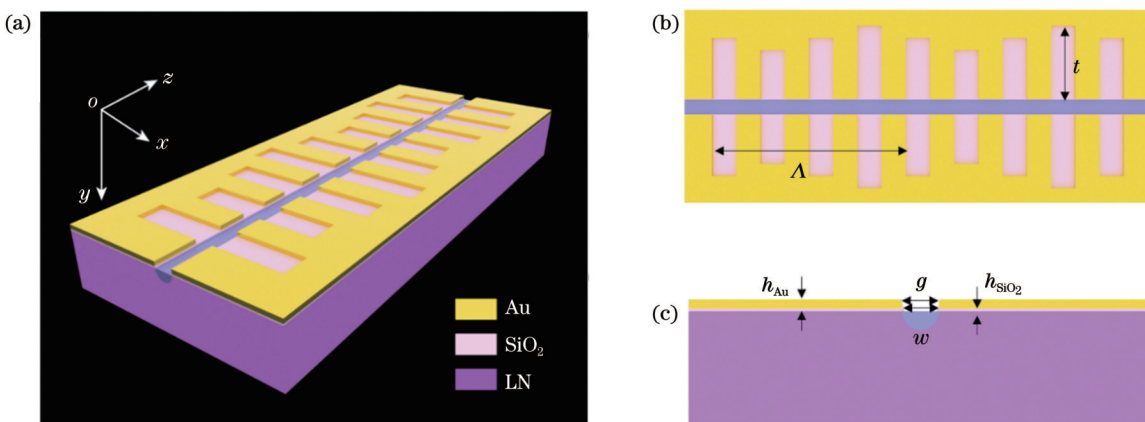


图1 光波-太赫兹波混合波导示意图。(a)整体示意图;(b)俯视图;(c)正视图

Fig. 1 Schematic of light-wave-terahertz wave hybrid waveguide. (a) Overall schematic; (b) top view; (c) front view

尽管退火质子交换波导的折射率差值较小,属于弱束缚波导,但是与薄膜铌酸锂(TFLN)波导相比,其与单模光纤的模场匹配较好,可以在端面耦入更高功率的激光,有利于进行高效非线性转化,产生更大功率的太赫兹波,便于探测。质子交换的概念是Jackel等于1982年最先提出的^[33],其基本原理在于,在质子交换过程中,熔融酸中的氢离子(H^+)会取代铌酸锂表层的锂离子(Li^+),因此改变了铌酸锂晶体的结构,从而增大非常光(e光)的折射率。其基本化学过程可由下面的化学式描述:



常用热退火来避免质子交换波导中非 α 相晶体的晶格常数与 LiNbO_3 基底的晶格常数差别很大的问题。通过退火的波导质子交换区折射率变化量在水平和竖直方向上的关系可以分离变量,其中竖直方向(y 方向)上近似满足高斯分布,水平方向(x 方向)则近似满

足误差函数,并且与 SiO_2 掩模的开口宽度 w 有关,表达式可以写为

$$\Delta n_e(\lambda, x, z) = \Delta n_p(\lambda) \cdot f(x) \cdot g(y), \quad (2)$$

式中: $f(x)$ 和 $g(y)$ 分别表示波导在水平和竖直方向上的折射率分布; Δn_e 为e光的折射率增量; Δn_p 为 $x=0, y=0$ 处的折射率增量。

$$\left\{ \begin{array}{l} f(x) = \frac{\operatorname{erf}\left(\frac{w/2+x}{D_x}\right) + \operatorname{erf}\left(\frac{w/2-x}{D_x}\right)}{2\operatorname{erf}\left(\frac{w}{2D_x}\right)} \\ g(y) = \exp\left[-\frac{y^2}{(D_e + D_y)^2}\right] \end{array} \right. . \quad (3)$$

只要知道质子扩散深度 D_e 、水平方向退火深度 D_x 和竖直方向退火深度 D_y ,就可以知道退火质子交换波导的折射率分布。使用COMSOL Multiphysics

软件进行近红外光波本征模式的仿真模拟,得到光波模场的空间分布和对应的有效折射率,并计算得到群折射率。为了使通信波段光波和太赫兹波之间的有效模式面积最小,非线性耦合系数最大,本

实验选用 X 切铌酸锂。当 SiO_2 掩模的开口宽度 w 为 $5.5 \mu\text{m}$ 时,1550 nm 波长附近的近红外光波 TE 基模的电场分布和群折射率 n_g 随波长的变化如图 2 所示。

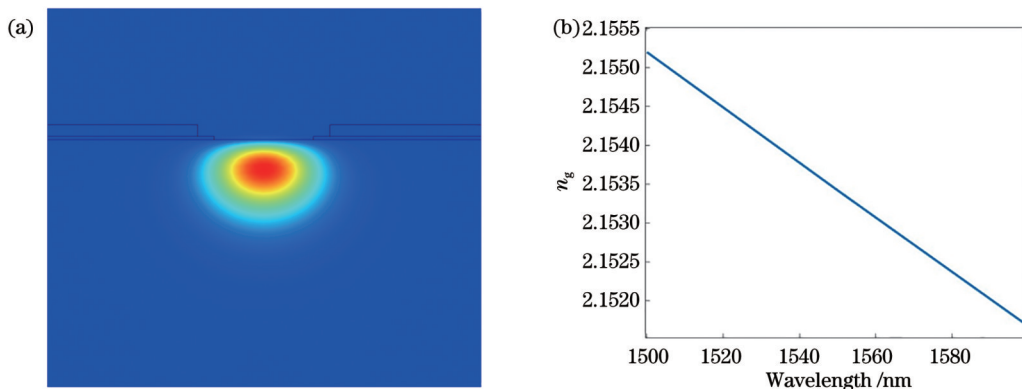


图 2 近红外光波模场分布与色散。(a) 1550 nm TE 基模电场分布;(b) 近红外光波群折射率随波长的变化

Fig. 2 Mode field distribution and dispersion of near-infrared light waves. (a) Distribution of 1550 nm TE mode electric field; (b) variation in near-infrared light group refractive index with wavelength

考虑一个实际波导 DFG 过程,太赫兹波频率 $\omega_T = \omega_1 - \omega_2$,其中 ω_1 为泵浦光频率, ω_2 为信号光频率,相互作用区域为 $0 \leq z \leq L$ 。如果泵浦光和信号光向太赫兹频率 ω_T 部分转换的能量非常少,电场强度沿传播方向均匀分布,根据耦合波方程,DFG 太赫兹波强度^[34]可表示为

$$I_T = |A_T|^2 = \left(\frac{\mu_0}{\epsilon_0} \right)^{1/2} \frac{2I_1 I_2 d_{\text{eff}}^2 \omega_T^2}{c^2 n_1 n_2 n_T} \frac{\sin^2 \left(\frac{1}{2} \Delta k L \right)}{\left(\frac{1}{2} \Delta k L \right)^2}, \quad (4)$$

式中: d_{eff} 为光波与太赫兹波之间的有效非线性耦合系数; n_1 为泵浦光的有效折射率; n_2 为信号光的有效折射率; n_T 为产生的闲频太赫兹波的有效折射率; Δk 为相位失配量; μ_0 为真空磁导率; ϵ_0 为真空介电常数; I_1 为泵浦光强度; I_2 为信号光强度; c 为真空中的光速。

相位匹配对于高效率 DFG 至关重要,它确保生成的差频波在非线性介质长度方向上干涉相长,而不是相互抵消。近红外光波与太赫兹波的波长差别较大,难以在同种材料中进行相位匹配。LiNbO₃ 材料中常用的相位匹配技术包括双折射相位匹配、非共线相位匹配^[35]、模式相位匹配、准相位匹配^[36]等。光学超晶格就是二阶非线性光学系数受到周期性调制的材料,能够用于激光的准相位匹配非线性频率转换^[37]。

实际上,准相位匹配技术的内涵远不止通过周期极化使得畴反转,还可以通过其他的周期性结构,例如亚波长的超材料,来提供倒格矢,补偿非零波矢失配。本文通过周期性的金属超晶格来提供倒格矢,实现准相位匹配。这种周期性的金属锯齿结构也是较好的低损耗太赫兹波导的选择^[38-39]。差频过程的准相位匹配条件为

$$\beta_1 - \beta_2 = \beta_T + qK, \quad (5)$$

式中: q 为准相位匹配的阶数, $q=0$ 时即为普通的相位匹配; β_1 为泵浦光传播常数; β_2 为信号光传播常数; β_T 为差频产生的太赫兹的传播常数; K 为一维波导共线准相位匹配引入的倒格矢。考虑到太赫兹波频率与近红外光波频率相差较大, $\omega_1 \approx \omega_2$,再加上群折射率的定义 $n_g = c \frac{d\beta}{d\omega} \approx c \frac{\beta_1 - \beta_2}{\omega_T}$,则准相位匹配条件可化为

$$n_g = n_T + \frac{2\pi qc}{\Lambda \omega_T}, \quad (6)$$

式中: n_g 为近红外光波的群折射率; n_T 为太赫兹波的有效折射率; Λ 为引入的周期性金属超晶格的大周期。

经计算验证,光波折射率受到上层金属的影响较小。因此,可以通过改变上层金属波导的结构调控太赫兹波的有效折射率,使得光波和太赫兹波满足准相位匹配条件[式(6)]。一阶准相位匹配时,取 $q=1$ 。为了增大非线性耦合系数,满足 1550 nm(193.4 THz)附近的近红外光波和 0.4 THz 附近的太赫兹波一阶准相位匹配条件,减小光波和太赫兹波的损耗,需要对金属超晶格的结构进行特殊设计。一个金属超晶格大周期 Λ 中有 m 个小周期,引入周期性调制,这样做能使得能带折叠,打开带隙。太赫兹电场大部分位于空气中而不是铌酸锂中,因此太赫兹波的传输损耗较小。

对于镜面对称的金属超晶格,如果只看其中一个小周期的原胞,其可分为对称耦合和反对称耦合两个基模。经计算发现,对称耦合模式在中间铌酸锂波导处的能量更局域,相应的交叠积分更大,非线性相互作用更强。反对称模式的电场在中间部分基本上全部抵消。后面如果没有特殊说明,金属超晶格的基模就是

指对称模式。使用 COMSOL Multiphysics 软件进行仿真,在太赫兹波段,金属选用理想电导体。

与常规的光子晶体一样^[40-42],金属超晶格的色散出现在靠近带边的位置,色散曲线的斜率趋近于 0,这样就可以实现极低的光子传播速度,实现慢光效应。这里的太赫兹波速度指群速度 v_{gT} ,即能量的传播速度。

由计算结果可知,对太赫兹波色散影响最大的结构参数是锯齿深度 t 和间距 g 。为了尽量不影响模场压缩程度,将调制加在锯齿深度 t 上:

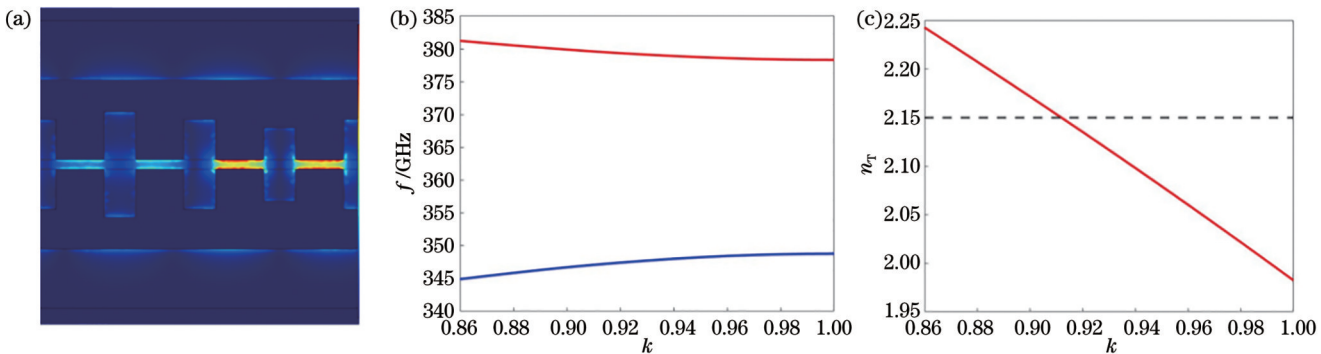


图 3 太赫兹波模场分布与色散。(a)金属超晶格太赫兹模场分布;(b)金属超晶格色散;(c)准相位匹配点

Fig. 3 Mode field distribution and dispersion of terahertz waves. (a) Metal superlattice terahertz mode field distribution; (b) metal superlattice dispersion; (c) quasi-phase matching point

这种经过调制的金属超晶格在 0.4 THz 附近的色散和准相位匹配点如图 3(b)、(c)所示,其中 k 为波数,图 3(c)中虚线与实线的交点即为准相位匹配点。这种周期性结构破坏了空间平移对称性,使得超晶格满足布拉格条件,从而引发布拉格衍射。在光子晶体中,这种衍射效应会导致光子在某些频率范围内无法在晶格中传播,形成禁能带,即图 3(b)中的带隙。越靠近带边,慢光效应^[43]越明显,太赫兹波的群折射率越大,这样就能获得更大的非线性耦合系数。

制备混合集成波导过程中,铌酸锂基片选用直径为 7.62 cm(3 inch)、厚为 0.5 mm 的光波导级 X 切铌酸锂基片,采用苯甲酸(C_6H_5COOH)作为质子源。制备退火质子交换波导的工艺流程主要包括:1)样品前处理与表面准备;2) SiO_2 薄膜生长;3)光刻过程(正胶);4)干法刻蚀过程;5)样品切割与清洗;6)质子交换过程;7)退火处理。基于金属超晶格的太赫兹波导的制备工艺流程主要包括:1)样品前处理与表面准备;2)套刻过程(负胶);3)蒸镀金属;4)剥离过程;5)抛光过程。

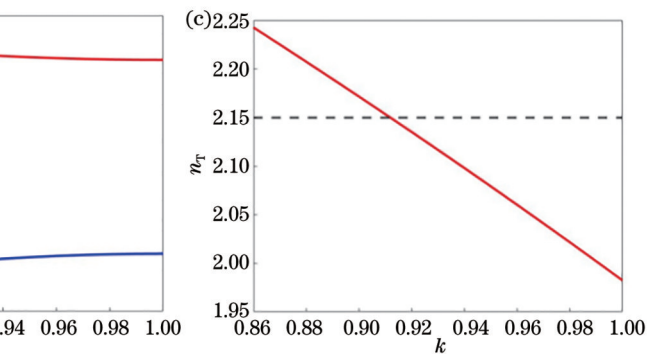
通过上述步骤,可以确保样品表面及其结构的制备精度,便于近红外光的端面耦入与低损耗传播,为后续的太赫兹信号探测提供了坚实的基础。这些工艺都是很成熟的,而且无需电子束光刻(EBL),无需极化,成本可控。

3 理论计算与讨论

对于铌酸锂混合集成波导,在这种准相位匹配条

$$t_i = t_0 \left\{ 1 + D_p \sin \left[\frac{2\pi}{m} (i-1) \right] \right\}, \quad (7)$$

式中: D_p 为调制深度; i 为锯齿序号。为了同时具有较大的非线性耦合系数和较小的传输损耗,不妨假设结构参数的正弦调制引起非线性系数的正弦调制——弱耦合,选择一个大周期包含 4 个小周期(即 $m=4$)。经过优化比较,金属超晶格波导的调制参数取 $t_0=25 \mu m$ 、 $D_p=0.2$,在其准相位匹配点,太赫兹电场模分布如图 3(a)所示。



件下,超晶格的非线性耦合系数 κ_s 随 z 变化,且具有周期性: $\kappa_s(z) = \kappa_s(z + \Lambda)$,其具体表达式为

$$\kappa_s(z) = \kappa_0 \exp \left[i \int_0^z \delta \kappa_T(\xi) d\xi \right] = \sum_m g_m \exp(i G_m z), \quad (8)$$

式中: κ_0 为非线性耦合系数; $\delta \kappa_T$ 为相位失配函数; ξ 为积分变量; g_m 为傅里叶系数; G_m 为第 m 阶傅里叶展开式对应的倒格矢。考虑实际波导结构并进行归一化,太赫兹波的非线性耦合系数 κ_T 可表示为

$$\kappa_T(z) = \frac{\omega_T}{2 \sqrt{W_1 W_2 W_T}} \iint_A \mathbf{e}_T^* \cdot \epsilon_0 \boldsymbol{\chi}^{(2)}(\omega_T) : \mathbf{e}_1 \mathbf{e}_2^* dx dy, \quad (9)$$

式中: \mathbf{e}_1 、 \mathbf{e}_2 和 \mathbf{e}_T 分别为泵浦光、信号光和闲频太赫兹的本征模场; W_1 、 W_2 和 W_T 为对应的本征波导模式功率; $\boldsymbol{\chi}^{(2)}$ 为二阶非线性系数;“*”表示复共轭; A 为模场面积。近红外光波的本征功率为

$$\begin{cases} W_1 \approx \frac{1}{2} \epsilon_0 c n_1 \iint_A |\mathbf{e}_1|^2 dx dy \\ W_2 \approx \frac{1}{2} \epsilon_0 c n_2 \iint_A |\mathbf{e}_2|^2 dx dy \end{cases} \circ. \quad (10)$$

由于太赫兹场强沿着传播方向(z 方向)并不均匀分布,对于太赫兹波,有

$$W_T = \frac{\Omega_T}{A} v_{gT}, \quad (11)$$

式中: v_{gT} 为太赫兹波的群速度; Ω_T 为一个周期内包含的能量,可表示为

$$\Omega_T = \frac{1}{4} \iint dx dy \int_0^A (\epsilon |\mathbf{e}_T|^2 + \mu_0 |\mathbf{h}_T|^2) dz. \quad (12)$$

将式(10)~(12)代入式(9), 可得

$$\kappa_T(z) = \frac{2d_{33}\sqrt{\Lambda n_{gT}}}{c\sqrt{n_1n_2c}} \times \frac{\iint_{NL} e_{1x}(x, y) e_{2r}^*(x, y) e_{Tr}^*(x, y, z) dx dy}{\sqrt{\Omega_T \iint_A |\mathbf{e}_1(x, y)|^2 dx dy \iint_A |\mathbf{e}_2(x, y)|^2 dx dy}}. \quad (13)$$

从式(13)可以看出,除了压缩模场面积,提高光波和太赫兹波的能量密度和交叠积分可以增大非线性耦合系数,利用慢光效应增大太赫兹波的群折射率 n_{gT} ,

也能增大非线性耦合系数 κ_T ,进而增大非线性转换效率 $\eta = I_T/(I_1 I_2)$ 。

根据式(13),在金属超晶格波导的一个大周期 A 内,其非线性耦合系数 $\kappa_T(z)$ 的实部和虚部随长度 z 的变化如图4(a)所示,其非线性耦合系数明显大于太赫兹波在直金属波导中传播的非线性耦合系数。对非线性耦合系数进行傅里叶变换后,其一阶分量也较高,说明在非线性光学差频过程中,很大部分能量积累下来,如图4(b)所示。傅里叶变换得到的一阶分量即为有效非线性耦合系数。非线性转换效率随传输长度的变化如图4(c)所示,传输0.5 cm左右,非线性转换效率达到饱和值 $3.6 \times 10^{-7} \text{ W}^{-1}$ 。

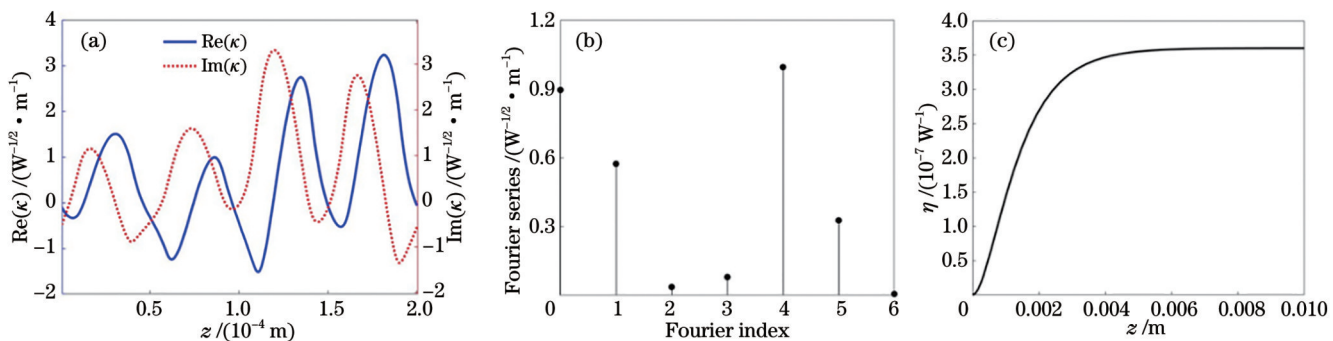


图4 非线性耦合系数。(a)一个周期内非线性耦合系数的实部和虚部随长度的变化;(b)非线性耦合系数的傅里叶变换;(c)非线性转换效率随长度的变化

Fig. 4 Nonlinear coupling coefficient. (a) Variation in the real and imaginary parts of the nonlinear coupling coefficient over one period with length; (b) Fourier transform of nonlinear coupling coefficient; (c) variation in conversion efficiency with length

由于材料、结构和波长不同,很难直接比较非线性光学差频产生太赫兹波的转换效率。太赫兹波在不考虑声子极化激元共振效应的情况下传输0.5 cm,基于混合集成波导理论实现了 $3.6 \times 10^{-7} \text{ W}^{-1}$ 的转换效率。

此外,本文方法无需周期极化和非共线相位匹配,更便于集成和应用。表1所示为基于铌酸锂混合波导的THz-DFG设计与其他基于铌酸锂设计的太赫兹源的比较。

表1 部分基于铌酸锂的代表性太赫兹源转换效率比较
Table 1 Comparison of selected representative THz conversion efficiency

Type	Working frequency / THz	Continuous or pulsed	Length / cm	Conversion efficiency / W^{-1}	Note
APELN	0.379	Continuous	0.5	3.6×10^{-7}	Theory (this work)
TFLN	3	Continuous	3	3.5×10^{-4}	Theory ^[44]
TFLN	30	Continuous	1	9.16×10^{-6}	Theory ^[45]
PPLN	1.5	Pulsed	2	2.0×10^{-9}	Experiment ^[46]
PPLN	2.14	Pulsed	10	2.1×10^{-4}	Theory ^[47]
APPLN	60.8	Continuous	3	1.1×10^{-9}	Theory ^[48]
Bulk LN	7.5	Continuous	Bulk	1.5×10^{-7}	Experiment ^[49]
Bulk LN	<1	Pulsed	Bulk	1.03×10^{-2}	Experiment ^[35]

Notes: APELN—annealed proton exchange lithium niobate; TFLN—thin-film lithium niobate; PPLN—periodically poled lithium niobate; APPLN—aperiodically poled lithium niobate; Bulk LN—bulk lithium niobite.

4 结 论

从非线性光学的差频理论与公式推导出发,设计

了一种将退火质子交换铌酸锂波导和金属超晶格太赫兹波导混合集成的高效非线性差频太赫兹源。通过设计波导结构,利用带边慢光效应的独有特性,在准相位

匹配的情况下,从理论上克服了差频产生过程中相位失配和光学-太赫兹波之间弱非线性相互作用方面的挑战。设计出一种室温、连续、高效、集成化、低噪声、易于调制的相干太赫兹源。值得注意的是,所提出的非线性混合波导制备工艺成熟、操作简单,无需 EBL,无需极化。所使用的金属超晶格结构其实不必拘泥于特定的函数形式,可以用机器学习、最优化等方法寻找最适合的场强分布,可以利用连续谱中的准束缚态(Q-BIC)共振模式等特殊模式,还可以在波导两端镀膜形成微腔,进一步提升非线性转换效率。这种混合集成的方法不仅可以用到光学差频中,也可以用到其他的非线性光学过程中。另外,所提方法不局限于铌酸锂这一材料,可以用到其他体系的光子芯片中。

参 考 文 献

- [1] Dang S, Amin O, Shihada B, et al. What should 6G be? [J]. Nature Electronics, 2020, 3(1): 20-29.
- [2] Federici J, Moeller L. Review of terahertz and subterahertz wireless communications[J]. Journal of Applied Physics, 2010, 107(11): 111101.
- [3] Woodward R M, Wallace V P, Arnone D D, et al. Terahertz pulsed imaging of skin cancer in the time and frequency domain [J]. Journal of Biological Physics, 2003, 29(2): 257-259.
- [4] Akyildiz I F, Jornet J M, Han C. Terahertz band: next frontier for wireless communications[J]. Physical Communication, 2014, 12: 16-32.
- [5] Nagatsuma T, Ducournau G, Renaud C C. Advances in terahertz communications accelerated by photonics[J]. Nature Photonics, 2016, 10: 371-379.
- [6] Jepsen P U, Cooke D G, Koch M. Terahertz spectroscopy and imaging—modern techniques and applications[J]. Laser & Photonics Reviews, 2011, 5(1): 124-166.
- [7] Lewis R A. A review of terahertz sources[J]. Journal of Physics D, 2014, 47(37): 374001.
- [8] Jiang Y Q, Li H Q, Zhang X Q, et al. Promoting spintronic terahertz radiation via Tamm plasmon coupling[J]. Photonics Research, 2023, 11(6): 1057-1066.
- [9] Zhang S, Cui Y W, Wang S J, et al. Nonrelativistic and nonmagnetic terahertz-wave generation via ultrafast current control in anisotropic conductive heterostructures[J]. Advanced Photonics, 2023, 5(5): 056006.
- [10] 宫玉彬, 周庆, 田瀚文, 等. 基于电子学的太赫兹辐射源[J]. 深圳大学学报(理工版), 2019, 36(2): 111-127.
- [11] Gong Y B, Zhou Q, Tian H W, et al. Terahertz radiation sources based on electronics[J]. Journal of Shenzhen University (Science and Engineering), 2019, 36(2): 111-127.
- [12] Fülöp J A, Tzortzakis S, Kampfrath T. Laser-driven strong-field terahertz sources[J]. Advanced Optical Materials, 2020, 8(3): 1900681.
- [13] Zhu D, Shao L B, Yu M J, et al. Integrated photonics on thin-film lithium niobate[J]. Advances in Optics and Photonics, 2021, 13(2): 242-352.
- [14] 孙军, 郝永鑫, 张玲, 等. 铌酸锂晶体及其应用概述[J]. 人工晶体学报, 2020, 49(6): 947-964.
- [15] Sun J, Hao Y X, Zhang L, et al. Brief review of lithium niobate crystal and its applications[J]. Journal of Synthetic Crystals, 2020, 49(6): 947-964.
- [16] Luo Q, Bo F, Kong Y F, et al. Advances in lithium niobate thin-film lasers and amplifiers: a review[J]. Advanced Photonics, 2023, 5(3): 034002.
- [17] 熊霄, 曹启韬, 肖云峰. 铌酸锂集成光子器件的发展与机遇[J]. 物理学报, 2023, 72(23): 234201.
- [18] Xiong X, Cao Q T, Xiao Y F. Thin-film lithium niobate photonic integrated devices: advances and opportunities[J]. Acta Physica Sinica, 2023, 72(23): 234201.
- [19] Qi Y F, Li Y. Integrated lithium niobate photonics[J]. Nanophotonics, 2020, 9(6): 1287-1320.
- [20] 徐光耀, 马晓飞, 盛冲, 等. 采用人工表面等离激元电极的慢光铌酸锂电光调制器[J]. 光学学报, 2023, 43(19): 1923001.
- [21] Xu G Y, Ma X F, Sheng C, et al. Slow-light lithium niobate electro-optic modulators with spoof surface plasmon polaritons electrodes[J]. Acta Optica Sinica, 2023, 43(19): 1923001.
- [22] Ravi K, Huang W R, Carbajo S, et al. Limitations to THz generation by optical rectification using tilted pulse fronts[J]. Optics Express, 2014, 22(17): 20239-20251.
- [23] Yang K H, Richards P L, Shen Y R. Generation of far-infrared radiation by picosecond light pulses in LiNbO₃[J]. Applied Physics Letters, 1971, 19(9): 320-323.
- [24] Pendry J B, Holden A J, Robbins D J, et al. Magnetism from conductors and enhanced nonlinear phenomena[J]. IEEE Transactions on Microwave Theory and Techniques, 1999, 47(11): 2075-2084.
- [25] Liu Z W, Lee H, Xiong Y, et al. Far-field optical hyperlens magnifying sub-diffraction-limited objects[J]. Science, 2007, 315(5819): 1686.
- [26] Fang N, Lee H, Sun C, et al. Sub-diffraction-limited optical imaging with a silver superlens[J]. Science, 2005, 308(5721): 534-537.
- [27] Schurig D, Mock J J, Justice B J, et al. Metamaterial electromagnetic cloak at microwave frequencies[J]. Science, 2006, 314(5801): 977-980.
- [28] Sheng C, Liu H, Wang Y, et al. Trapping light by mimicking gravitational lensing[J]. Nature Photonics, 2013, 7: 902-906.
- [29] Li G X, Zhang S, Zentgraf T. Nonlinear photonic metasurfaces [J]. Nature Reviews Materials, 2017, 2(5): 17010.
- [30] Koshelev K, Tonkaev P, Kivshar Y. Nonlinear chiral metaphotonics: a perspective[J]. Advanced Photonics, 2023, 5(6): 064001.
- [31] Lapine M, Shadrivov I V, Kivshar Y S. Colloquium: nonlinear metamaterials[J]. Reviews of Modern Physics, 2014, 86(3): 1093-1123.
- [32] Suchowski H, O'Brien K, Wong Z J, et al. Phase mismatch-free nonlinear propagation in optical zero-index materials[J]. Science, 2013, 342(6163): 1223-1226.
- [33] Kauranen M, Zayats A V. Nonlinear plasmonics[J]. Nature Photonics, 2012, 6(11): 737-748.
- [34] McDonnell C, Deng J H, Sideris S, et al. Functional THz emitters based on Pancharatnam-Berry phase nonlinear metasurfaces[J]. Nature Communications, 2021, 12: 30.
- [35] Ma X F, Wang N Y, Cao R Z, et al. Optical to terahertz frequency conversion using near zero-index nonlinear hybrid waveguides[J]. Optics Continuum, 2024, 3(5): 682-690.
- [36] Chen C Y, Chen Y P, Fang Z F, et al. Hybrid material integration for active photonic applications[J]. APL Photonics, 2024, 9(3): 030903.
- [37] Kuneva M, Tonchev S, Pashtapanska M, et al. Proton exchange in Y-cut LiNbO₃[J]. Materials Science in Semiconductor Processing, 2000, 3(5/6): 581-583.
- [38] Liu Y, Zhong K, Wang A Q, et al. Optical terahertz sources based on difference frequency generation in nonlinear crystals[J]. Crystals, 2022, 12(7): 936.
- [39] Wu X J, Kong D Y, Hao S B, et al. Generation of 13.9-mJ terahertz radiation from lithium niobate materials[J]. Advanced Materials, 2023, 35(23): 2208947.
- [40] Zhu S N, Zhu Y Y, Ming N B. Quasi-phase-matched third-harmonic generation in a quasi-periodic optical superlattice[J]. Science, 1997, 278(5339): 843-846.
- [41] 闵乃本, 朱永元, 祝世宁, 等. 介电体超晶格的研究[J]. 物理,

- 2008, 37(1): 1-10.
Min N B, Zhu Y Y, Zhu S N, et al. Dielectric superlattices[J]. Physics, 2008, 37(1): 1-10.
- [38] Liu H, Genov D A, Wu D M, et al. Magnetic plasmon propagation along a chain of connected subwavelength resonators at infrared frequencies[J]. Physical Review Letters, 2006, 97(24): 243902.
- [39] Garcia-Vidal F J, Fernández-Domínguez A I, Martín-Moreno L, et al. Spoof surface plasmon photonics[J]. Reviews of Modern Physics, 2022, 94(2): 025004.
- [40] Tang H N, Du F, Carr S, et al. Modeling the optical properties of twisted bilayer photonic crystals[J]. Light: Science & Applications, 2021, 10(1): 157.
- [41] Zhou W D, Zhao D Y, Shuai Y C, et al. Progress in 2D photonic crystal Fano resonance photonics[J]. Progress in Quantum Electronics, 2014, 38(1): 1-74.
- [42] Yang Y, Roques-Carmes C, Kooi S E, et al. Photonic flatband resonances for free-electron radiation[J]. Nature, 2023, 613(7942): 42-47.
- [43] Baba T. Slow light in photonic crystals[J]. Nature Photonics, 2008, 2: 465-473.
- [44] Yang J W, Wang C. Efficient terahertz generation scheme in a thin-film lithium niobate-silicon hybrid platform[J]. Optics Express, 2021, 29(11): 16477-16486.
- [45] Yoshioka V, Jin J C, Zhen B. Coherent FIR/THz wave generation and steering via surface-emitting thin film lithium niobate waveguides[J]. Optics Express, 2024, 32(1): 639-651.
- [46] Hamazaki J, Ogawa Y, Kishimoto T, et al. Conversion efficiency improvement of terahertz wave generation laterally emitted by a ridge-type periodically poled lithium niobate[J]. Optics Express, 2022, 30(7): 11472-11478.
- [47] Ding Y J. Efficient generation of far-infrared radiation from a periodically poled LiNbO₃ waveguide based on surface-emitting geometry[J]. Journal of the Optical Society of America B, 2011, 28(5): 977-981.
- [48] Li Z Y, Sun X Q, Zhang H T, et al. High-efficiency terahertz wave generation in aperiodically poled lithium niobate by cascaded difference frequency generation[J]. Journal of the Optical Society of America B, 2020, 37(8): 2416-2422.
- [49] de Regis M, Bartalini S, Ravaro M, et al. Room-temperature continuous-wave frequency-referenced spectrometer up to 7.5 THz[J]. Physical Review Applied, 2018, 10(6): 064041.

Lithium Niobate Hybrid Integrated Waveguide Nonlinear Terahertz Source

Wang Nengyu, Xue Feihong, Ma Xiaofei, Sheng Chong, Xiao Yanling, Zhu Shining, Liu Hui*

National Laboratory of Solid State Microstructures, Collaborative Innovation Center of Advanced Microstructures, School of Physics, Nanjing University, Nanjing 210093, Jiangsu, China

Abstract

Objective Terahertz (THz) wireless communication is considered a strong candidate for 6G networks. Currently, the rapid development of terahertz science and technology faces significant bottlenecks. One of the main reasons is that traditional electronic devices used for generating radio waves can no longer meet the demands for low-noise terahertz wave generation and high-speed modulation. This challenge impedes the widespread deployment and commercialization of terahertz technology across various application fields. Among the many nonlinear optical materials for generating terahertz waves, lithium niobate stands out due to its excellent electro-optic, acousto-optic, and nonlinear properties, as well as its ultra-wide transparent window and relatively high refractive index. These attributes have made it one of the most versatile and attractive photonic materials. Furthermore, metamaterials, which feature sub-wavelength artificially designed microstructures, exhibit extraordinary physical properties not found in natural materials. This provides unprecedented flexibility in the manipulation of optical materials. We aim to apply the design philosophy of metamaterials to develop a terahertz source on a lithium niobate platform that can meet the demands of 6G communication.

Methods Starting from the theory of nonlinear optical difference frequency generation and the derivation of coupled-wave equations, we employ COMSOL Multiphysics software for simulation and numerical calculations to design a hybrid waveguide that integrates optical and terahertz waves. For the first time, we integrate an annealed proton-exchanged lithium niobate optical waveguide with a metallic superlattice terahertz waveguide for difference frequency generation of terahertz waves. The signal light and pump light in the near-infrared communication band propagate through the lithium niobate waveguide, inducing a nonlinear difference frequency process to generate THz waves. The waveguide structure is designed to compress the mode field. By optimizing the structural parameters of the metallic superlattice terahertz waveguide, we not only guide the propagation of the generated THz waves but also compress the THz optical field to sub-wavelength dimensions, thereby enhancing the spatial overlap with the electric field distribution of the lithium niobate optical waveguide. Additionally, we control the propagation and dispersion of the terahertz waves. This theoretically achieves quasi-phase matching, enhances the group refractive index of the THz waves, and further amplifies the nonlinear effects through the slow light effect. The difference frequency-generated THz waves are ultimately radiated into free space

at the end of the waveguide.

Results and Discussions Based on a hybrid integrated waveguide that combines an annealed proton-exchanged lithium niobate waveguide with a metallic superlattice terahertz waveguide, nonlinear difference frequency generation produces 0.379 THz terahertz waves. The theoretical nonlinear conversion efficiency reaches up to $3.6 \times 10^{-7} \text{ W}^{-1}$. The mode field distribution and dispersion of the near-infrared light transmitted through the annealed proton-exchanged lithium niobate waveguide are presented (Fig. 2). The mode field distribution and dispersion of the metallic superlattice terahertz waveguide are also provided (Fig. 3). The near-infrared and terahertz waves meet the first-order quasi-phase matching condition for difference frequency generation. The variation of the real and imaginary parts of the nonlinear coupling coefficient within one period with length is shown in the Fig. 4(a). The variation of nonlinear conversion efficiency with length is depicted as well [Fig. 4(c)]. Theoretically, this leads to a room-temperature, continuous, efficient, integrated, low-noise, and easily modulated coherent terahertz source. Notably, the fabrication process for our proposed nonlinear hybrid waveguide is mature and simple, eliminating the need for electron beam lithography (EBL) or polarization.

Conclusions In this paper, we begin with the theory and formulas of nonlinear optical difference frequency generation to design an efficient nonlinear difference frequency terahertz source. This design integrates annealed proton exchange lithium niobate waveguides with metallic superlattice terahertz waveguides. By designing the waveguide structure and leveraging the unique characteristics of edge slow-light effects, we theoretically address challenges related to phase mismatch and weak nonlinear interactions between optical and terahertz waves under quasi-phase-matching conditions. Theoretically, this approach presents a room-temperature, continuous, high-efficiency, integrated, low-noise, and easily modulated coherent terahertz source. The metallic superlattice structure is not confined to a specific functional form. Various methods, including machine learning and optimization, can be employed to identify the most suitable field distribution. Additionally, by coating the ends of the waveguide to create a microcavity, the nonlinear conversion efficiency can be further enhanced. This hybrid integration method is not only applicable to optical difference frequency generation but also to other nonlinear optical processes. Moreover, it is not restricted to lithium niobate but can be used in photonic chips of other systems.

Key words lithium niobate; waveguide; metamaterial; difference frequency; terahertz